Robust Merged Bound States in the Continuum for Ultrahigh-Q Optical Sensing

Peilin Zhao[1,3], Jiahang Liu[1,3], Zhengyang Li[2], Peilin Chen[3*]
[1]School of Materials Science and Engineering, Hebei University of Technology, Tianjin, 300401, China
[2]School of Science, Hebei University of Technology, Tianjin, 300401, China
[3]Department of Materials Science and Engineering, University of Arizona, Tucson, AZ 85721, USA
Corresponding author: Peilin Chen (e-mail: 3484733342@qq.com).

ABSTRACT Symmetry-protected bound states in the continuum (SP-BIC), characterized by theoretically vanishing radiation loss, provide an effective platform for realizing high-Q metamaterial systems and improving optical sensing performance. Nevertheless, conventional isolated SP-BIC modes generally exhibit limited Q-factor enhancement and require delicate symmetry perturbations for excitation, which imposes stringent fabrication constraints and reduces practical feasibility. This paper proposes a BIC merging strategy to enhance resonant Q factors, maintaining ultrahigh Q values under considerable symmetry breaking. A double-layer silicon nanohole metamaterial is designed to merge SP-BIC and Fabry–Pérot BIC by adjusting interlayer spacing, which modifies the radiative characteristics of the initial SP-BIC. Numerical simulations reveal that the merged BIC configuration achieves a three-order-of-magnitude enhancement in the Q factor compared with isolated counterparts. The BIC-based structure presented here displays a refractive index sensitivity of 230 nm/RIU, and the FOM surpasses 4.8×10^5 RIU^{-1}, which is much higher than the conventional isolated BIC structure. This work offers an effective solution for developing high-performance optical sensing devices based on merged BIC resonances.

INDEX TERMS Symmetry-protected BIC; Fabry–Pérot BIC; merged BIC; ultrahigh Q factor; refractive index sensing

I. INTRODUCTION

BOUND States in the Continuum (BIC) belong to a unique class of optical resonances. Although their frequency lies in the radiation continuum, they can effectively eliminate radiative leakage, so they possess theoretically unlimited quality factors. In addition, BIC can ideally prevent energy leakage into external radiation channels, resulting in a dark optical state. Nevertheless, practical implementations generally convert ideal BIC into quasi-bound (q-BIC) states, because of finite dimensions, intrinsic material absorption, and symmetry perturbations, and their Q factors remain considerably large despite being finite. Quasi-bound states have wide extensive applications in fields such as high-sensitivity sensing, low-threshold lasers, narrowband filtering, and nonlinear optics. Their advantages lie in the strong local field effect [1], narrowband response [2–4], and controllability of radiation coupling [2, 3].

Depending on the underlying radiation cancellation mechanism, optical BIC can generally be classified into two categories: symmetric protection type and asymmetric type. Symmetry-protected BIC utilize modal symmetry mismatch to inhibit radiation coupling, where symmetry perturbations convert them into q-BIC states. Conversely, asymmetric BIC, such as Friedrich-Wintgen BIC and Fabry-Perot BIC (FP-BIC), realize radiation cancellation via interference among multiple resonant modes, offering enhanced structural tunability and improved fabrication robustness. Therefore, it has a great promise for reconfigurable and integrated photonic platforms [4-9].

Owing to the remarkable capability of BIC in reducing radiative losses, conventional BIC-based architectures can realize ultrahigh-Q resonances, which is crucial for advancing the functionality of photonic devices. However, insufficient interaction between resonant modes remains a major challenge, restricting further enhancement of the quality factor to some extent. To overcome this limitation, researchers have developed various approaches to optimize the properties of BIC-based systems. Zhang et al. demonstrated ultrahigh-Q quasi-BIC modes with enhanced sensing capability by introducing controlled perturbations around a photonic crystal plate. They used mode expansion theory and standing wave guidance conditions to engineer asymmetric environments to control the radiation channel, thus boosting the Q factor while increasing the response to surrounding refractive-index variations [10]. Wang et al. designed an all-silicon metasurface without polarization dependence to achieve quasi-BIC resonance in the THZ band with a Q factor reaching 1049, exceeding previous reports by over three orders of magnitude [11]. Fang et al. achieved a q-BIC resonance featuring an enhanced quality factor and strong electromagnetic confinement through an asymmetric dielectric grating design constructed from a low refractive index material. This design is not only able to produce symmetrically protected quasi-BIC in the visible light range, but also substantially improves the capability of refractive index detection [12]. Ruan et al. designed a hybrid photonic architecture integrating a grating layer with a multilayer configuration, and analyzed its energy bands and BIC positions using transmission matrix theory. It has been shown that the multilayer structure of the grating can deliver superior Q-factor performance compared with conventional grating structures [13]. Wang et al. used a tandem deep neural network approach to realize inverse-designed BIC resonances with Q factors spanning from several hundred to beyond one hundred thousand in the range of 400 to 1200 nm. This strategy significantly improves the design efficiency of high-Q resonant structures and demonstrates the potential of deep learning techniques for advanced nanophotonic sensing applications. [14]. Recently, Gao and colleagues put forward a design approach for metasurfaces. This approch is founded on degenerate guided-mode resonances integrated with BIC coalescence. By optimizing lattice parameters to minimize radiation loss, they managed to attain merged degenerate BIC states. Moreover, they also uncovered the coupling mechanism between guided-mode resonances and Fabry–Pérot background modes These findings offer novel perspectives on the advancement of high-Q photonic interaction platforms. However, conventional symmetry-protected BIC setups generally demand extremely minor structural disturbances to reach ultrahigh Q factors, resulting in considerable challenges for experimental realization and practical applications. [15].

Here, we propose a method for enhancing resonance quality by incorporating BIC features into the photonic structure, allowing the system to upload an extremely high Q factor, even when there are substantial symmetry deviations. Specifically, a double-layer dielectric grating structure is designed to simultaneously support symmetry-protected BIC and Fabry–Pérot-type BIC modes under normal incidence. By tuning the separation distance between the two layers, the two BIC states can be merged into a single resonance state. Results from numerical simulations indicate that the merged-BIC structure attains a Q-factor improvement of approximately three orders of magnitude compared to separate BIC configurations, accompanied by enhanced modal confinement and strengthened resonant interactions. For refractive-index sensing, the proposed device exhibits excellent sensing capability. It reaches a wavelength sensitivity of 230 nm/RIU and the FOM surpassing 4.8×10^5 RIU^{-1}, which is significantly higher than that of conventional isolated-BIC configurations, demonstrating its potential for highly sensitive detection and practical sensing applications.

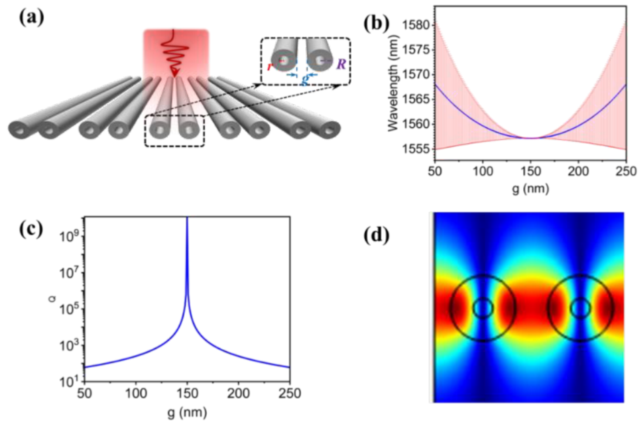

FIGURE 1. Circular-hole nanowire metasurface and offset-dependent eigenmode characteristics. (a) Schematic diagram of the circular hole nanowires metasurface, where $R = 150$ nm, the inner radius $r = 45$ nm, and the period $P = 900$ nm. (b) The evolution of the eigenmode spectrum as a function of the varying offset parameter g. The error bars represent the corresponding radiation leakage. (c) Variation of the quality factor as a function of g. (d) Electric field distribution at $g = 150$ nm.

II. MATERIALS AND METHODS

In this study, we first investigate a dielectric metasurface unit composed of two identical silicon nanorods with circular holes, as illustrated in Fig. 1(a), where g represents the lateral spacing between the two nanorods. The nanowire radius and aperture radius are set to $R = 150$ nm and $r = 45$ nm, respectively. To evaluate the optical characteristics of the proposed structure, three-dimensional finite-element simulations were performed using COMSOL Multiphysics to calculate the eigenfrequency response. To simulate the optical characteristics of silicon within the near-infrared wavelength spectrum, a refractive index of 3.5 was employed. The whole structure is situated in an atmospheric environment and stimulated under standard illumination circumstances. In periodic photonic setups, especially those that uphold time-reversal and spatial inversion symmetry, SP-BIC states can occur at high-symmetry locations (such as Γ) when the resonant frequency remains below the diffraction threshold. Such modes exhibit suppressed radiation because of the incompatibility between their modal symmetry and available radiation channels, thereby avoiding interaction with free-space radiation modes. For the designed metasurface configuration, the ideal BIC state evolves into a q-BIC mode through deliberate structural asymmetry which introduces finite radiative coupling. By tuning the nanorod separation parameter g, the magnitude of symmetry perturbation can be controlled, as shown in Figure 1(b). For the completely symmetric configuration ($g = 150$ nm), the system supports an intrinsic mode featuring negligible radiation leakage, corresponding to a symmetry-protected BIC state, while the red curve represents the associated radiation loss. Figure 1(c) illustrates the emergence of the symmetry-protected BIC state and the trend of its Q factor with varying g, demonstrating that disruption of structural symmetry significantly affects the optical performance and confirming the strong dependence of SP-BIC on structural symmetry. For the electric-field distribution shown in Fig. 1(d) indicates strong electromagnetic confinement in the gap region between the two circular-hole nanowires at $g = 150$ nm. The enhanced electromagnetic intensity inside the nanowire gap originates from near-field interaction between adjacent elements, confirming the localized field enhancement mechanism of the proposed structure.

Next, a second identical metasurface layer is introduced to form a bilayer structure that supports FP-BIC modes. In this architecture, the two vertically coupled arrays interact with each other and establish a Fabry–Pérot-type resonance system. Such a double-layer arrangement introduces more complicated resonance interactions and provides an effective platform for investigating BIC formation and related properties. To further clarify the physical origin of BIC formation in this system, the interaction between the two resonance modes is further analyzed using Temporal Coupled-Mode Theory (TCMT). The relevant Hamiltonian can be presented in the following manner: [16]

$$H = \begin{pmatrix} \omega_0 & \kappa \\ \kappa & \omega_0 \end{pmatrix} - i\gamma \begin{pmatrix} 1 & e^{i\psi} \\ e^{i\psi} & 1 \end{pmatrix} \tag{1}$$

In this context, ω and γ symbolize the resonant frequency and the rate of radiation loss corresponding to each mode, respectively. The coupling factor κ quantifies the intensity of the near-field interaction between the two resonant modes. Meanwhile, the phase disparity resulting from propagation is given by $\varphi = \kappa d$, where k signifies the transverse wave vector and d indicates the distance separating the two modes. For two magnetically coupled modes that display the same phase correlation, the eigenvalues of the Hamiltonian can be obtained as described below.

$$\omega = \omega_0 + \kappa - i\Upsilon\left(e^{-i\psi}\right) \tag{2}$$

When the difference in phase amounts to an integer multiple of π, the eigenfrequency stays entirely real. This real eigenfrequency corresponds to the creation of a BIC state in which radiative loss is curbed. Consequently, by adjusting the separation distance d to control the accumulated phase difference ψ, the FP-BIC can be achieved under suitable phase-matching circumstances. Figure 2(a) presents the schematic representation of the proposed double-layer circular-hole nanowire configuration, wherein the symbol d represents the vertical separation between two layers, which determines the coupling strength and resonance wavelength variation. Figure 2(b) illustrates how the coupled-mode Q factor varies with the interlayer spacing d for different offset parameters g reveals that structural symmetry breaking has a pronounced influence on optical characteristics, highlighting the sensitivity of SP-BIC modes to symmetry conditions. These findings indicate that precise regulation of g and d is crucial for controlling SP-BIC and FP-BIC interactions in the bilayer configuration, resulting in stronger Fano resonances and narrower spectral responses, and providing a promising approach for realizing stable high-Q hybrid photonic systems.

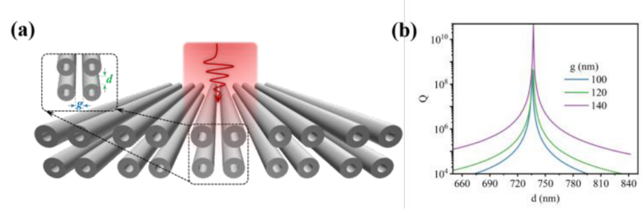

FIGURE 2. Double-layer metasurface configuration and spacing-dependent Q-factor characteristics. (a) Illustration of the proposed double-layer metasurface architecture. (b) Dependence of the Q factor on spacing d under different g values.

III. RESULTS

To elucidate the evolution of two localized resonances toward mode merging, we first investigated how two independent BIC modes interact under specific conditions and eventually merge into a new resonant state. This transition is accompanied by resonance-frequency variation and substantial modification of the Q factor. Figure 3(a) depicts the evolution of multiple BIC modes into a single BIC mode by varying the interlayer spacing d (along with changes in the offset g). As d increases, the two FP-BIC modes gradually converge toward the central SP-BIC mode, eventually evolving into a single ultrahigh-Q resonance when d reaches 738 nm. This mode coalescence originates from coherent interference and coupling interactions among distinct BIC states, highlighting that precise control and tuning of the modes can be achieved by fine adjustments of structural parameters, allowing the realization of extremely large Q factors. Figure 3(b) presents a comparative analysis of the Q-factor evolution for the merged BIC structure (depicted by the blue curve) and the isolated SP-BIC structure (depicted by the red curve) across the full spectrum of g values. The findings reveal that, over a broad parameter range, the Q-factor sustained by the merged BIC configuration is markedly superior to that of the isolated SP-BIC, demonstrating an enhancement exceeding three orders of magnitude.

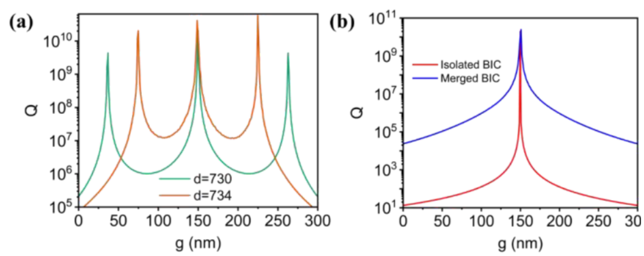

FIGURE 3. BIC coalescence process and its influence on Q-factor improvement. (a) Schematic diagram of the merging process of BIC patterns. (b) Comparison of the merged BIC and the isolated BIC on the Q-factor.

To investigate the coupling behavior and tunable characteristics between SP-BIC and FP-BIC modes, two-dimensional transmission spectra were systematically calculated by varying the structural displacement g and incident wavelength. As depicted in Fig. 4(a), for the isolated BIC structure, upholding perfect geometric symmetry facilitates the creation of a typical symmetry-safeguarded BIC state that has minimal radiative loss. As the offset parameter

g undergoes an increase, the symmetry inherent in the structure is gradually disrupted. This disruption results in the originally trapped BIC mode becoming coupled with external radiation pathways. Subsequently, this mode evolves into a leaky resonance with a narrow line-width, which exhibits distinct Fano features. In contrast, as depicted in Fig. 4(b), the merged-BIC configuration maintains an ultranarrow resonance linewidth and enhanced Q-factor characteristics even under significant symmetry perturbations. This robustness originates from the coalescence of multiple BIC states, leading to substantial reduction of radiative leakage.

To quantitatively evaluate and compare the resonance properties, the simulated transmission spectra were analyzed through Fano-line-shape fitting, allowing accurate extraction of the corresponding Q factors [17].

$$T(\lambda) = A + B\left(q + \frac{\lambda - \lambda_0}{\frac{\Gamma}{2}}\right)^2 \Big/ \left[1 + \left(\frac{\lambda - \lambda_0}{\frac{\Gamma}{2}}\right)^2\right] \quad (3)$$

In Equation (3), the symbols A and B signify fitting factors. The variable q denotes the spectral asymmetry parameter. Meanwhile, λ and Γ denote the resonance wavelength and the full width at half-maximum, respectively. The transmission spectra of the isolated and merged BIC configurations with an offset of $g = 146$ nm are presented in Figures 4(c) and 4(d). The calculation the calculated results indicate that the isolated BIC configuration achieves an extracted Q factor of 1478, while the merged-BIC system substantially elevates the Q factor to 3.12×10^6, corresponding to an enhancement of nearly three orders of magnitude. This significant enhancement verifies the capability of the BIC merging approach to suppress radiative losses and improve electromagnetic confinement. It should be noted that the Q factors reported in this work correspond to idealized radiative Q factors obtained from periodic full-wave simulations. In practical devices, the measurable total Q factor may be further limited by material absorption, fabrication-induced scattering, finite-size effects, substrate leakage, and external coupling losses.

Notably, tuning the lateral displacement g back to the symmetric configuration can markedly increase the resonance quality factor. Nevertheless, in conventional isolated-BIC systems, ultrahigh-Q operation can only be obtained within a very narrow range around $g = 0$. Figure 5 summarizes the calculated Q-factor evolution of BIC configurations under various offset parameters g. For the isolated BIC configuration, a Q factor on the order of 10^4 is obtained only at $g = 155$ nm, suggesting that achieving ultrahigh-Q resonances requires strict fabrication accuracy. Due to fabrication tolerances in nanofabrication, maintaining such strict symmetry conditions is difficult in practical fabrication. In comparison, the merge-BIC configuration preserves large Q factors across a significantly wider offset spectrum, indicating enhanced structural stability and enhanced resilience to manufacturing variations. This robustness is highly beneficial for practical photonic integration and applications relying on high-Q resonances.

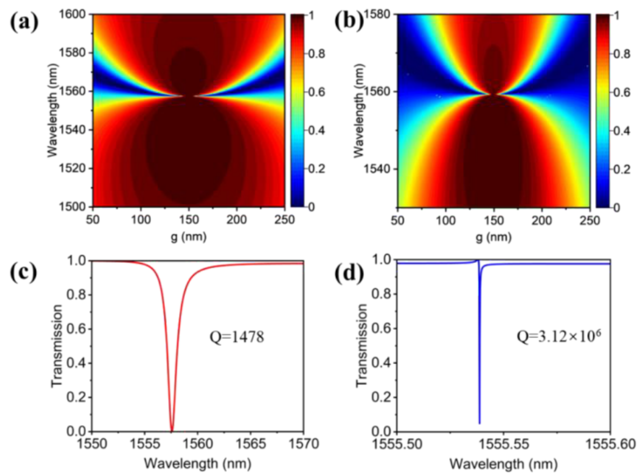

FIGURE 4. Far-field spectral characteristics of isolated and merged BIC configurations. Respectively, (a) and (b) illustrate the two-dimensional transmission profiles of isolated and merged BIC configurations as a function of both wavelength and lateral displacement g. Meanwhile, (c) and (d) show the relevant one-dimensional transmission spectrometry obtained from (a) and (b) when the value of g is set at 146 nm.

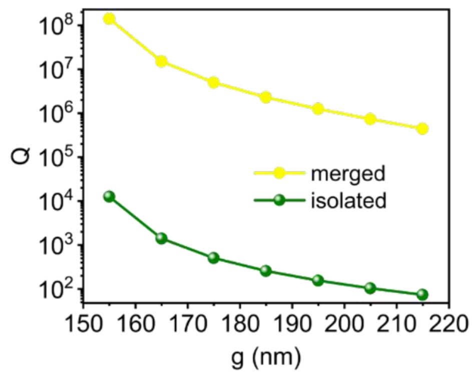

FIGURE 5. Illustrates the distribution of Q-factors in different parameter Spaces for BIC merge versus isolate designs.

Next, we analyze how the merged BIC states influence the sensing capability of the proposed system, where the refractive-index sensitivity (S) and figure of merit (FOM) are commonly used metrics to assess the sensing performance of the proposed structure. The sensitivity measures the spectral displacement of the resonance caused by alterations in the refractive index of the surrounding environment and can be represented as [18].

$$S = \frac{\Delta\lambda}{\Delta n} \quad (4)$$

Here, $\Delta\lambda$ denotes the resonance wavelength displacement, whereas Δn corresponds to the variation of the surrounding refractive index. Figure 6(a) and 6(b) illustrate the transmission evolution of individual and merged BIC configurations subjected to different surrounding refractive-index conditions, respectively. It is observed that both configurations present pronounced Fano-like spectral profiles accompanied by evident wavelength redshifts when the surrounding refractive index increases. Such spectral displacement originates primarily from the change in optical propagation wavelength inside the sensing environment caused by the increased refractive index of the surrounding environment, thus inducing a redshift of the resonance position to maintain the phase-matching condition. To quantitatively analyze this phenomenon, the position of the resonance wavelength versus the refractive index is plotted and fitted linearly in Figure 6(c) and 6(d), respectively. The linear fitting results indicate that the individual BIC sensor achieves a sensitivity value of 234 nm/RIU with respect to refractive-index variation. The slight discrepancy in sensitivity between these two configurations can be attributed to the strong localization of the localized optical fields supported by the nanostructure, resulting in relatively weak interaction with the surrounding medium.

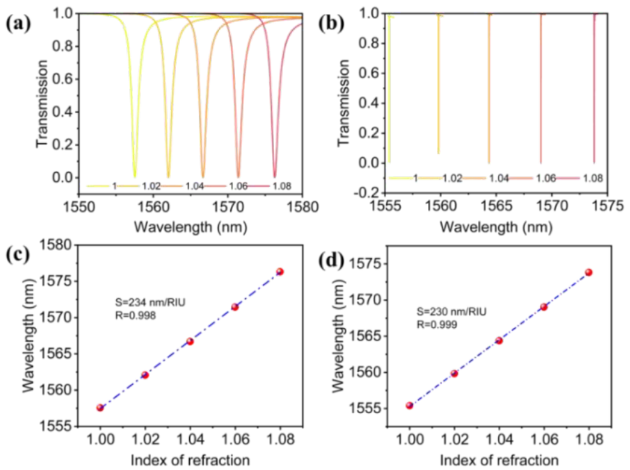

FIGURE 6. Refractive-index-dependent transmission characteristics of isolated and merged BIC configurations. Respectively, (a) and (b) illustrate the evolution of transmission spectra for the isolated and merged BIC configurations, as the surrounding refractive indices change. For the two configurations, figures (c) and (d) respectively show how the resonance wavelengths rely on the refractive index of the surrounding.

Furthermore, the figure of merit (FOM) offers an extra crucial parameter for assessing the sensing performance, which can be defined as [19].

$$FOM = S/FWHM \tag{5}$$

where FWHM represents the resonance linewidth measured at half of the maximum intensity, extracted from the spectral fitting process using Eq. (3). The calculated values of the FOM for the two configurations are shown in Figures 7(a) and 7(b). The calculated results reveal that the individual BIC structure reaches a maximum FOM of 253 RIU^{-1}, whereas the merge -BIC sensor exhibits a substantially enhanced FOM, with a maximum value of 4.8×10^5 RIU^{-1}. This remarkable enhancement demonstrates that BIC coalescence greatly improves the sensing figure of merit, leading to superior sensing capability owing to the greatly narrowed resonance linewidth, despite the comparable sensitivity values.

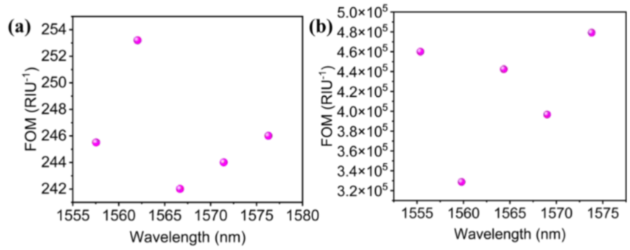

FIGURE 7. Comparison of the figure of merit between isolated and merged BIC structures. The FOM values of the isolated BIC structure and the merged BIC structure are represented by (a) and (b), respectively.

IV. CONCLUSIONS

In summary, we present a strategy for enhancing the resonance quality factor by triggering the interaction between the SP-BIC and FP-BIC modes. This strategy enables the system to preserve ultrahigh-Q resonances despite substantial symmetry perturbations, while maintaining stable performance over a broad parameter range. The proposed sensor achieves an outstanding figure of merit (FOM), demonstrating promising prospects for high-resolution sensing and accurate detection applications. In addition, the proposed design provides flexible structural tunability and strong tolerance against variations in symmetry-breaking parameters, while remaining highly feasible for practical implementation, making it particularly attractive for precision detection and measurement scenarios including environmental monitoring, biochemical analysis, and integrated photonic platforms.

ACKNOWLEDGMENT

This work was supported by the College Students' Innovation and Entrepreneurship Training Program Projects of Hebei Province (Grant No: S202510080024).

REFERENCES

[1] N. Sun, W. Zhang, H. Yuan, and X. Zhang, "Boundary-localized many-body bound states in the continuum," *Commun. Phys.*, vol. 7, p. 299, 2024.

[2] Y. Wang, Z. Ju, Z. Liu, Y. Zhang, X. Song, K. Ren, J. Bai, R. Chen, J. Dong, Y. Bai, and T. Fu, "Enhancement and sensing performance of ultra-narrowband induced circular dichroism in achiral nanohole arrays based on bound states in the continuum," *ACS Appl. Mater. Interfaces*, vol. 18, pp. 8658–8669, 2026.

[3] X. Zong, L. Li, and Y. Liu, "Bound states in the continuum enabling ultra-narrowband perfect absorption," *New J. Phys.*, vol. 25, Art. no. 023020, 2023.

[4] L. Li, L. Cui, X. Zong, and Y. Liu, "Multinarrowband perfect absorption with bound states in the continuum for sensing application," *IEEE Sens. J.*, vol. 24, pp. 4400–4406, 2024.

[5] Y. Chen, G. Guo, S. Liu, S. Yin, W. Huang, and W. Zhang, "Quasi-bound states in the continuum induced by supercell coupling," *Opt. Express*, vol. 31, pp. 18807–18823, 2023.

[6] I. A. M. Al-Ani, K. As'Ham, L. Huang, A. E. Miroshnichenko, and H. T. Hattori, "Enhanced strong coupling of TMDC monolayers by bound state in the continuum," *Laser Photonics Rev.*, vol. 15, Art. no. 2100240, 2021.

[7] T. C. Meiler, Y. Wang, S. Srivastava, G. Adamo, R. Paniagua-Domínguez, A. I. Kuznetsov, and C. Soci, "Spectral tuning of perovskite laser via microheaters," *Nano Lett.*, vol. 25, pp. 9695–9701, 2025.

[8] R. Kanyang, C. Fang, Q. Yang, Y. Shao, G. Han, Y. Liu, and Y. Hao, "Electro-optical modulation in high Q metasurface enhanced with liquid crystal integration," *Nanomaterials*, vol. 12, Art. no. 3179, 2022.

[9] F. Lei, S. Wang, L. Wu, K. Wen, J. Zhu, J. Yang, Y. Qin, Ultra-high quality-factor enhancement via merged bound states in the continuum for

high-performance optical sensing, *Journal of Applied Physics*, 139 (2026) 053105.

[10] C. Damgaard-Carstensen, T. Yezekyan, M. L. Brongersma, and S. I. Bozhevolnyi, “Highly efficient, tunable, electro-optic, reflective metasurfaces based on quasi-bound states in the continuum,” *ACS Nano*, vol. 19, pp. 11999–12006, 2025.

[11] H. Zhong, T. He, Y. Meng, and Q. Xiao, “Photonic bound states in the continuum in nanostructures,” *Materials*, vol. 16, Art. no. 7112, 2023.

[12] C. Wang, R. Wang, X. Cheng, X. Hu, and C. Wang, “Passively broadband tunable dual circular dichroism via bound states in the continuum in topological chiral metasurface,” *ACS Nano*, vol. 18, pp. 18922–18932, 2024.

[13] J. Zhang, X. Ma, Y. Liu, H. Lu, and K. Yu, “Ultrahigh-Q and ultrasensitive quasi-bound states in the continuum via asymmetric environment engineering of a photonic crystal slab,” *Opt. Express*, vol. 33, pp. 48227–48243, 2025.

[14] P. Wang, F. He, J. Liu, F. Shu, B. Fang, T. Lang, X. Jing, and Z. Hong, “Ultra-high-Q resonances in terahertz all-silicon metasurfaces based on bound states in the continuum,” *Photon. Res.*, vol. 10, pp. 2743–2750, 2022.

[15] Z.-Z. Fang, H.-L. Xu, J.-Y. Su, J.-Y. Zhou, and Z.-M. Meng, “Ultra-high-Q and ultra-sensitive refractive index sensing in low refractive index dielectric gratings based on bound states in the continuum,” *J. Opt. Soc. Am. B*, vol. 41, pp. 98–104, 2024.

[16] Y. Ruan, Y. Li, Z. Hu, J. Wang, and Y. Wang, “Strong resonance response with ultrahigh quality factor in grating-multilayer systems based on quasi-bound states in the continuum,” *Sci. Rep.*, vol. 12, Art. no. 21471, 2022.

[17] L. Wang, W. Wang, Q. Dong, L. Wang, and L. Gao, “Deep learning enabled inverse design of bound states in the continuum with ultrahigh Q factor,” *J. Opt. Soc. Am. B*, vol. 41, pp. A146–A151, 2024.

[18] Y. Gao, J. Ge, Z. Gu, L. Xu, X. Shen, and L. Huang, “Degenerate merging BICs in resonant metasurfaces,” *Opt. Lett.*, vol. 49, pp. 6633–6636, 2024.

[19] C. W. Hsu, B. Zhen, A. D. Stone, J. D. Joannopoulos, and M. Soljačić, “Bound states in the continuum,” *Nat. Rev. Mater.*, vol. 1, Art. no. 16048, 2016.

[20] F. Lei, S. Wang, L. Wu, and Y. Qin, “Dual-channel sensing technology with ultrahigh FOM enhanced by TMOKE,” *IEEE Sens. J.*, vol. 25, pp. 16027–16033, 2025.

[21] F. Lei, S. Wang, L. Wu, K. Wen, and Y. Qin, “Coupling of SPR and guided mode resonances for TMOKE enhancement and its application in sensing,” *Opt. Commun.*, vol. 592, Art. no. 132278, 2025.

[22] F. Lei, L. Li, P. Li, and Y. Liu, “Nanopore arrays with TMOKE-enhanced high-performance sensing,” *J. Opt.*, vol. 26, Art. no. 065003, 2024.